An integral formulation for fluid-structure interaction in hemodynamics

Umberto Iemma[1] & Giuseppe Pontrelli[2]
[1]*Dip. di Ingegneria Meccanica e Industriale*
Università degli Studi Roma Tre, Italy
E-mail: u.iemma@uniroma3.it
[2]*Istituto per le Applicazioni del Calcolo*
CNR - Roma, Italy
E-mail: g.pontrelli@iac.cnr.it

Abstract

To investigate the pulsatile flow in an artery, a new mathematical formulation for the study of three-dimensional flow within an elastic tube is presented. The linearized differential equations governing the fluid flow are recast as a boundary integral representation and coupled with the wall motion. The response of the fluid-wall system to a pressure pulse is studied by using a Laplace transform and by examining the solution in the frequency domain. Much attention is paid to the boundary conditions on the surfaces limiting the domain of the problem. The results of some numerical simulations, showing the characteristic frequencies of the fluid-structure system, prove the effectiveness of such a technique.

1 Introduction

The flow of a fluid in a compliant tube has received much attention because of its relevance in the applications, particularly in hemodynamics [1]. Specifically, the fluid-structure interaction is of the primary interest in modelling blood flow, because of the arterial wall remodelling process and the subsequent altered flow pattern in pathological states. Wave propagation in arteries has been examined experimentally, but *in vivo* studies in vascular flows are difficult, expensive and limited to easily accessible arteries. Theoretical studies and computational modelling offer an attractive method of investigation [2],[3].

The fluid *blood* and the *arterial* structure constitute an intrinsically coupled system. Its dynamics is adequately described by a set of differential equations which should be solved by a fully coupled method [4]. Because of many physiological and clinical implications, several differential models of fluid-structure interaction have been developed and analyzed [5].

A boundary integral method will be used here to solve the blood–vessel system and will be adapted for the specific features of the problem at hand. Boundary integral methods have been extensively used in solving the interaction of elastic boundaries with both external and internal flows in aeroelastic and acoustoelastic problems [6–10]. The main advantage of such a formulation stems from the redefinition of a three-dimensional differential problem into an integral form defined on a 2D manifold (the domain boundary) embedded in the 3D space. This results in a reduction of the computational effort required for the numerical solution of the coupled system. Similar techniques have been widely used in the past for the analysis of fluid-structure interaction problems.

In the present application, such a technique is used to describe the flow pattern alteration due to a compliant structure. In particular, we deal with the internal flow of a liquid in an elastic tube, driven by a pulsatile forcing function. It is worth noting that such a point of view is somehow reversed with respect to the classical aeroelastic approach, where much attention is paid to the structural dynamics. The main objective of this study is to get an insight of the complex relationship between arterial pressure, wall deformation and flow field in a large arterial vessel. Neglecting fluid viscosity, our attention is focused on the harmonic response of the *fluid-wall* interacting system to a pulsatile inflow. Our ultimate goal is the prediction of the flow modification in presence of a prosthetic implantation or in pathological conditions.

The plan of this chapter is as follows. In sections 2 and 3 the mathematical description of the problem and the boundary integral formulation for the fluid flowing in an elastic tube is given in its general form. The resulting integro-differential equation is solved numerically by a zeroth-order boundary element method, and the pressure evaluated from the potential through the Bernoulli's theorem. Great attention is paid to the suitable boundary conditions to be imposed at the ends of the finite domain (sect. 4). The compliant wall is modelled as an elastic shell which deforms under the flow-induced loads. Many constitutive laws for the arterial wall are available in literature [11], [12] and, because of small deformations, a linear elastic material will be adopted here. The problem is addressed with a Galërkin approach and expressed in matrix form (sect. 5). Section 6 is devoted to the coupling between the structural and fluid equations. These are rewritten in the frequency domain through the Laplace transform and assembled to yield an algebraic system. Finally, the method is applied to the specific case of a thin-walled vascular segment and preliminary numerical results are presented and discussed in section 7. To validate the methodology, the formulation is here applied to a simple configuration, such as that of a straight cylindrical tube.

The presented results show the harmonic response of the fluid-structure system and predict the wave propagation velocity. The new formulation allows us to deal

with an arbitrary 3D geometry and, though limited to a linear structural operator, is shown to be an effective tool in the prediction of wave propagation phenomena in compliant vessels and deserves further investigation.

2 Mathematical formulation

Let us consider a homogeneous incompressible inviscid fluid of density ρ, flowing in a compliant tube of finite length. Let $\mathcal{V} \subset \Re^3$ be the volume occupied by the fluid. Its boundary $\mathcal{S}$ is constituted by the elastic wall of the arterial vessel (surface $\mathcal{S}^{\mathsf{w}}$) and by the inlet and outlet surfaces, $\mathcal{S}^{\mathsf{i}}$ and $\mathcal{S}^{\mathsf{o}}$. Therefore $\partial\mathcal{V} = \mathcal{S} = \mathcal{S}^{\mathsf{i}} \cup \mathcal{S}^{\mathsf{w}} \cup \mathcal{S}^{\mathsf{o}}$ (fig. 1). Henceforth, the superscript indexes i, w, and o refer to variables on $\mathcal{S}^{\mathsf{i}}, \mathcal{S}^{\mathsf{w}}, \mathcal{S}^{\mathsf{o}}$ respectively.

According to the Kelvin's theorem, an initially irrotational flow of such a fluid remains irrotational at all times. Thus, the velocity potential field $\phi(\mathbf{x}, t)$ is defined such that:

$$\mathbf{v}(\mathbf{x}, t) = \nabla\phi(\mathbf{x}, t) \tag{1}$$

with $\mathbf{v}$ the fluid velocity vector.

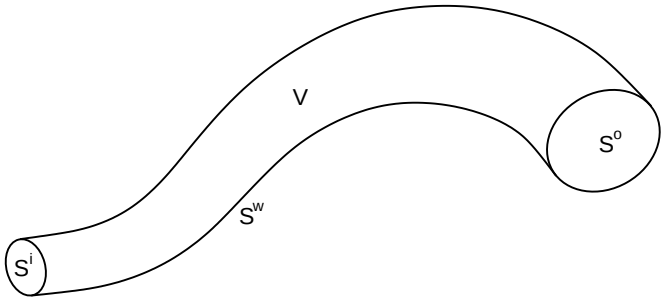

Figure 1: Sketch of the arterial segment with the surfaces $\mathcal{S}^{\mathsf{i}}$ (inlet), $\mathcal{S}^{\mathsf{w}}$ (elastic wall) , $\mathcal{S}^{\mathsf{o}}$ (outlet).

The continuity equation for incompressible flows $\nabla \cdot \mathbf{v} = 0$, is expressed in terms of the velocity potential as:

$$\nabla^2\phi = 0 \tag{2}$$

The above differential equation must be completed with suitable boundary conditions. On the surface $\mathcal{S}^{\mathsf{w}}$, the impermeability condition is imposed:

$$\frac{\partial\phi}{\partial n} := \nabla\phi \cdot \mathbf{n} = \mathbf{v}^{\mathsf{w}} \cdot \mathbf{n}, \qquad \text{on } \mathcal{S}^{\mathsf{w}} \tag{3}$$

with $\mathbf{v}^{\mathsf{w}}$ the wall velocity and $\mathbf{n}$ the inward normal. For the application considered here, $\mathbf{v}^{\mathsf{w}}$ is the time derivative of the elastic displacement $\mathbf{u}$, and the condition (3)

becomes:

$$\frac{\partial \phi}{\partial n} = \dot{\mathbf{u}} \cdot \mathbf{n} \tag{4}$$

(dot over a variable denotes time derivative).

On the inlet section $\mathcal{S}^{\text{i}}$ we assume the velocity to be a uniform known (typically periodic in time). Denoting $\mathbf{v}^{\text{i}}$ the incoming velocity, we have:

$$\nabla \phi \cdot \mathbf{n} = \mathbf{v}^{\text{i}}(t) \cdot \mathbf{n}, \qquad \text{on } \mathcal{S}^{\text{i}} \tag{5}$$

The boundary condition imposed at the section $\mathcal{S}^{\text{o}}$ needs a more careful discussion. The outflow rate is not an independent condition, but depends on the whole flow inside $\mathcal{V}$. The continuity equation (2) implies:

$$\int_{\mathcal{V}} \nabla^2 \phi \; d\mathcal{V}(\mathbf{x}) = 0$$

or, by the Gauss theorem:

$$\int_{\mathcal{V}} \nabla^2 \phi \; d\mathcal{V}(\mathbf{x}) = \int_{\mathcal{S}^{\text{i}}} \frac{\partial \phi}{\partial n} \, d\mathcal{S}(\mathbf{x}) + \int_{\mathcal{S}^{\text{o}}} \frac{\partial \phi}{\partial n} \, d\mathcal{S}(\mathbf{x}) + \int_{\mathcal{S}^{\text{w}}} \frac{\partial \phi}{\partial n} \, d\mathcal{S}(\mathbf{x}) = 0 \tag{6}$$

stating that, in the absence of mass sources inside $\mathcal{V}$, the mass is conserved and the total flow across its boundary is zero. This provides a compatibility condition between the inflow at $\mathcal{S}^{\text{i}}$, the normal velocity along $\mathcal{S}^{\text{w}}$ and the outflow at $\mathcal{S}^{\text{o}}$ holds. In Section 4, eqn. (6) will be used to yield the outflow condition.

Being interested in studying the perturbation of a fluid at rest having a constant reference pressure p_0, the relationship between velocity potential and pressure is given by the linearized Bernoulli theorem:

$$\dot{\phi} + \frac{p}{\rho} = \frac{p_0}{\rho} \tag{7}$$

3 The Boundary Integral Equation

The theoretical foundation of boundary integral methods is related to the *fundamental solution* of the governing equation, defined as the solution G of the so called *adjoint problem* [13]. For the Laplace equation (2) we have:

$$\nabla^2 G = \delta(\mathbf{x} - \mathbf{y}) \tag{8}$$

where $\delta(\mathbf{x} - \mathbf{y})$ is the Dirac δ function, representing an impulsive source located at $\mathbf{y}$. Equation (8) is completed by the vanishing condition at infinite distance from the perturbation point [6, 7]. The solution of eqn. (8) is:

$$G(\mathbf{x}, \mathbf{y}) = -\frac{1}{4\pi r} \quad \text{with} \quad r = ||\mathbf{x} - \mathbf{y}|| \tag{9}$$

It is worth noting that, although this problem deals with a bounded domain, we use expression (9) for G, which represents the *free–space Green function* for the

Laplacian operator. The boundary conditions associated with eqn. (2) are substantially different from those used in the adjoint problem (8), and the use of a Green function (*i.e.*, a fundamental solution satisfying the boundary conditions of the specific problem) could be considered a more suitable choice. Nevertheless, the derivation of such a Green function has often a higher level of difficulty than the solution of the original differential problem. An *a priori* recipe to identify the most convenient approach is not available, and the choice of the fundamental solution has to be made on the basis of the specific application (for details on the use of Green's functions see [13], [14], [15], [16]).

Multiplying eqn. (2) by G and eqn. (8) by ϕ, subtracting and integrating yields:

$$\int_{\mathcal{V}} \delta(\mathbf{x}-\mathbf{y})\phi(\mathbf{x})\ d\mathcal{V}(\mathbf{x}) = \int_{\mathcal{V}} \left(\phi\nabla^2 G - G\nabla^2\phi\right)\ d\mathcal{V}(\mathbf{x})$$

Recalling the properties of the Dirac δ function and applying the Gauss theorem, we finally obtain:

$$E(\mathbf{y})\phi(\mathbf{y},t) = \int_{\mathcal{S}} \left(G\frac{\partial\phi}{\partial n} - \phi\frac{\partial G}{\partial n}\right)\ d\mathcal{S}(\mathbf{x}), \tag{10}$$

where E is a domain function defined as:

$$E(\mathbf{y}) = \begin{cases} 1 \text{ if } \mathbf{y} \in \mathcal{V} \\ 0 \text{ if } \mathbf{y} \notin \bar{\mathcal{V}} \end{cases}$$

being the value on $\mathcal{S}$ derived through a limiting process (it can be proved $E(\mathbf{y}) = 1/2$ for regular points on smooth surfaces). The boundary integral eqn. (10) is a representation for the solution ϕ of the differential problem (2) and relates the value of the velocity potential at any point in $\mathcal{V}$ to the Cauchy data of the problem. For the problem under investigation, the Neumann boundary condition provides a value for $\partial\phi/\partial n$ on $\mathcal{S}$. Thus, in eqn. (10) the value of ϕ is unknown on the boundary. If $\mathbf{y} \in \mathcal{S}$, the above integral representation becomes a Boundary Integral Equation (BIE) for the velocity potential on $\mathcal{S}$ (for details, see [6],[13]). It is worth noting that, using the BIE approach, the original differential problem in $\Re^3$ is reduced to an integral equation on a two-dimensional manifold embedded into the $3D$ space. Once the solution ϕ has been obtained on $\mathcal{S}$, the same integral representation eqn. (10) may be used to get the value of the velocity potential at any point $\mathbf{y} \in \mathcal{V}$.

4 Numerical solution

The numerical solution of the above integral formulation is computed by means of a Boundary Element Method (BEM) (see [15]). Following this approach, the boundary $\mathcal{S}$ is partitioned into N surface elements (or panels) $\mathcal{S}_j$ (being $N = N^{\mathsf{i}} + N^{\mathsf{w}} + N^{\circ}$ and N^{i}, N^{w}, N° the number of the panels on $\mathcal{S}^{\mathsf{i}}$, $\mathcal{S}^{\mathsf{w}}$, $\mathcal{S}^{\circ}$ respectively) and a set of collocation points is chosen on each $\mathcal{S}_j$ to satisfy eqn.(10). This

procedure is known as the *collocation* method, and the choice of the surface elements shape and the number and the location of collocation points depend on the level of accuracy desired.

In the present work, we use the so called *zeroth order* formulation, in which the unknown is assumed to be piecewise constant. Despite its simplicity, this kind of discretization is able to describe complex geometries with a good level of detail. Higher order formulations have been developed to solve linear and nonlinear problems, with a faster convergence rate but at a higher computational cost [17].

Here, the surface elements are quadrilateral panels (triangular panels are treated as a limit case) described by a bilinear representation (fig. 2), the collocation points are located at the centers of the panels and all the functions are assumed to be constant–valued over each elements. The discretized form of eqn.(10) is:

$$E_n\,\phi_n = \sum_{j=1}^{N}\left[\chi_j \int_{S_j} G(\mathbf{x},\mathbf{y}_n)\; d\mathcal{S}(\mathbf{x}) - \phi_j \int_{S_j} \frac{\partial G}{\partial n}(\mathbf{x},\mathbf{y}_n)\; d\mathcal{S}(\mathbf{x})\right] \quad (11)$$

where subscripts indicate evaluation at the corresponding collocation point and $\chi = \partial\phi/\partial n$. Equation (11) can be rewritten as:

$$\frac{1}{2}\,\phi_n = \sum_{j=1}^{N} B^{\mathsf{i}}_{nj}\chi^{\mathsf{i}}_j + \sum_{j=1}^{N} B^{\mathsf{o}}_{nj}\chi^{\mathsf{o}}_j + \sum_{j=1}^{N} B^{\mathsf{w}}_{nj}\chi^{\mathsf{w}}_j + \sum_{j=1}^{N} C_{nj}\phi_j \quad (12)$$

with

$$B_{nj} = \int_{S_j} G(\mathbf{x},\mathbf{y}_n)\; d\mathcal{S}(\mathbf{x}), \qquad C_{nj} = -\int_{S_j} \frac{\partial G}{\partial n}(\mathbf{x},\mathbf{y}_n)\; d\mathcal{S}(\mathbf{x}) \quad (13)$$

Equation (12) represents a set of algebraic equations for the N unknowns ϕ_n and its matrix form is:

$$\frac{1}{2}\underline{\phi} = \mathsf{B}^{\mathsf{i}}\underline{\chi}^{\mathsf{i}} + \mathsf{B}^{\mathsf{o}}\underline{\chi}^{\mathsf{o}} + \mathsf{B}^{\mathsf{w}}\underline{\chi}^{\mathsf{w}} + \mathsf{C}\,\underline{\phi} \quad (14)$$

with B and C being the $N \times N$ matrices collecting the coefficients in (13) and underbar indicating column vectors.

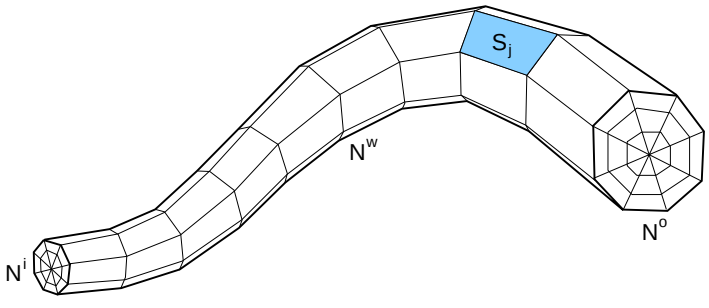

Figure 2: Boundary elements representation of the surface $\mathcal{S}$ (cfr. fig. 1).

Some consideration about the role of the first three terms on the right hand side is now given. First, the column vector containing the boundary conditions $\underline{\chi}$ is partitioned into the three $N \times 1$ vectors $\underline{\chi}^{\mathsf{i}}$, $\underline{\chi}^{\mathsf{o}}$, and $\underline{\chi}^{\mathsf{w}}$ as follows:

$$\underline{\chi} = \underline{\chi}^{\mathsf{i}} + \underline{\chi}^{\mathsf{w}} + \underline{\chi}^{\mathsf{o}} = \left\{ \begin{array}{c} \underline{\hat{\chi}}^{\mathsf{i}} \\ \cdots \\ 0 \\ \cdots \\ 0 \end{array} \right\} + \left\{ \begin{array}{c} 0 \\ \cdots \\ \underline{\hat{\chi}}^{\mathsf{w}} \\ \cdots \\ 0 \end{array} \right\} + \left\{ \begin{array}{c} 0 \\ \cdots \\ 0 \\ \cdots \\ \underline{\hat{\chi}}^{\mathsf{o}} \end{array} \right\} \tag{15}$$

where $\underline{\hat{\chi}}^{\mathsf{i}}, \underline{\hat{\chi}}^{\mathsf{w}}, \underline{\hat{\chi}}^{\mathsf{o}}$ are column vectors of length $N^{\mathsf{i}}, N^{\mathsf{w}}, N^{\mathsf{o}}$ respectively. Similarly, the coefficient matrices are defined as:

$$\mathsf{B}^{\mathsf{i}} = \left[\begin{array}{ccccc} \hat{\mathsf{B}}^{\mathsf{i}} & \vdots & 0 & \vdots & 0 \end{array} \right]$$

$$\mathsf{B}^{\mathsf{w}} = \left[\begin{array}{ccccc} 0 & \vdots & \hat{\mathsf{B}}^{\mathsf{w}} & \vdots & 0 \end{array} \right]$$

$$\mathsf{B}^{\mathsf{o}} = \left[\begin{array}{ccccc} 0 & \vdots & 0 & \vdots & \hat{\mathsf{B}}^{\mathsf{o}} \end{array} \right]$$

where $\hat{\mathsf{B}}^{\mathsf{i}}$, $\hat{\mathsf{B}}^{\mathsf{w}}$, $\hat{\mathsf{B}}^{\mathsf{o}}$ are, respectively, $N \times N^{\mathsf{i}}$, $N \times N^{\mathsf{w}}$, $N \times N^{\mathsf{o}}$ rectangular submatrices. Assuming a uniform velocity profile for the input and output sections, the discretized form of the eqn. (6) has the form:

$$A^{\mathsf{i}} \underline{\chi}^{\mathsf{i}} + A^{\mathsf{o}} \underline{\chi}^{\mathsf{o}} + \sum_{j=1}^{N^{\mathsf{w}}} A^{\mathsf{w}}_j \underline{\chi}^{\mathsf{w}}_j = 0 \tag{16}$$

where $A^{\mathsf{i}} = ||S^{\mathsf{i}}||$, $A^{\mathsf{o}} = ||S^{\mathsf{o}}||$ and $A^{\mathsf{w}}_j = ||S^{\mathsf{w}}_j||$. From eqn. (16) we obtain:

$$\underline{\chi}^{\mathsf{o}} = -\frac{1}{A^{\mathsf{o}}} \left(A^{\mathsf{i}} \underline{\chi}^{\mathsf{i}} + \sum_{j=1}^{N^{\mathsf{w}}} A^{\mathsf{w}}_j \chi^{\mathsf{w}}_j \right) = \underline{\chi}^{\mathsf{or}} + \mathsf{G}\, \underline{\chi}^{\mathsf{w}} \tag{17}$$

which gives the outflow as a function of inflow and wall–motion–induced normal velocity at the boundary $\mathcal{S}^{\mathsf{w}}$. The term $\underline{\chi}^{\mathsf{or}}$ on the right hand side of eqn. (17) corresponds to the outflow condition in the case of rigid walls, and is given by $-(A^{\mathsf{i}}/A^{\mathsf{o}})\, \underline{\chi}^{\mathsf{i}}$. The matrix G has the form:

$$\mathsf{G} = \left[\begin{array}{ccccc} \mathbf{0} & \vdots & \mathbf{0} & \vdots & \mathbf{0} \\ \cdots & \cdots & \cdots & \cdots & \cdots \\ \mathbf{0} & \vdots & -A^{\mathsf{w}}_j / A^{\mathsf{o}} & \vdots & \mathbf{0} \end{array} \right]$$

Substituting eqn. (17) into eqn. (14):

$$\left(\frac{1}{2}\mathsf{I} - \mathsf{C}\right) \underline{\phi} = \mathsf{B}^{\mathsf{i}} \underline{\chi}^{\mathsf{i}} + \mathsf{B}^{\mathsf{o}} \underline{\chi}^{\mathsf{or}} + (\mathsf{B}^{\mathsf{o}}\mathsf{G} + \mathsf{B}^{\mathsf{w}}) \underline{\chi}^{\mathsf{w}}. \tag{18}$$

The motion of the elastic boundary represents the coupling between the fluid and the mechanics of the structure. The boundary condition on the elastic walls given by eqn. (4) and evaluated in the j-th collocation point is:

$$\chi_j^{\mathsf{w}} = \dot{\mathbf{u}}_j \cdot \mathbf{n}_j \tag{19}$$

with $\mathbf{n}_j$ the unit normal to $\mathcal{S}_j^{\mathsf{w}}$. The latter equation provides the entries of vector $\underline{\chi}^{\mathsf{w}}$ as a function of the wall velocities at the BEM collocation points.

5 Dynamics of the elastic walls

Under the assumption of small elastic deformations, the wall dynamics is described within the framework of linear elasticity theory (see [18]). In such a context, the general form of the motion equation governing the structural dynamics is:

$$\rho_{\mathsf{w}}\, \ddot{\mathbf{u}} + \mathcal{L}\, \mathbf{u} = \mathbf{f} \tag{20}$$

where ρ_{w} is the wall density, $\mathcal{L}$ denotes the (self-adjoint) $3D$ linear elastic operator, and $\mathbf{f}(\mathbf{x}, t)$ is the forcing term due to the fluid flow.

A Galërkin approach is used to solve eqn. (20): the displacement $\mathbf{u}$ is expressed as a linear combination of vector functions $\boldsymbol{\varphi}_m(\mathbf{x})$ (the *trial functions*) with time dependent coefficients $a_m(t)$, and eqn. (20) is projected over the *test function* set. In this work, we choose both the trial and the test functions as the eigenfunctions of the operator $\mathcal{L}$, such that:

$$\mathcal{L}\, \boldsymbol{\varphi}_m = \rho_{\mathsf{w}}\, \lambda_m\, \boldsymbol{\varphi}_m, \tag{21}$$

λ_m being the corresponding eigenvalue. The theory of self-adjoint linear operators ensures that the $\boldsymbol{\varphi}_m$ are linearly independent and orthogonal *i.e.*,

$$\langle \boldsymbol{\varphi}_m, \boldsymbol{\varphi}_l \rangle_{\rho_{\mathsf{w}}} := \int_{\mathcal{V}^{\mathsf{w}}} \rho_{\mathsf{w}}\, \boldsymbol{\varphi}_m \cdot \boldsymbol{\varphi}_l \, d\mathcal{V}(\mathbf{x}) = \delta_{ml} \tag{22}$$

where $\mathcal{V}^{\mathsf{w}}$ is the volume of the elastic solid, and δ_{ml} is the Kronecker's function. The elastic displacement is expressed by the linear combination:

$$\mathbf{u}(\mathbf{x}, t) = \sum_{m=1}^{\infty} a_m(t)\, \boldsymbol{\varphi}_m(\mathbf{x}) \simeq \sum_{m=1}^{M} a_m(t)\, \boldsymbol{\varphi}_m(\mathbf{x}) \tag{23}$$

truncated to the order M. Substituting eqn. (23) into eqn. (20), projecting on the eigenfunction space, by means of eqns. (21) and (22), we have:

$$\ddot{a}_l(t) + \omega_l^2\, a_l(t) = e_l(t), \qquad l = 1, ..., M \tag{24}$$

where ω_l is the l^{th} eigenfrequency, and the *generalized* force e_l is the inner product between the l^{th} eigenfunction and the force due to the pressure perturbation

exerted by the fluid on the wall. In the present formulation, where the effects of viscosity are neglected, $\mathbf{f} = -(p - p_0)\delta(\eta)\mathbf{n}$, being δ the Dirac function and $\eta(\mathbf{x}) = 0$ the equation of the inner solid boundary. Hence:

$$\begin{aligned} e_l = \langle \mathbf{f}, \boldsymbol{\varphi}_l \rangle &= -\int_{\mathcal{V}^{\mathsf{w}}} (p - p_0)\, \delta(\eta)\ \mathbf{n} \cdot \boldsymbol{\varphi}_l\ d\mathcal{V}(\mathbf{x}) \\ &= -\int_{\mathcal{S}^{\mathsf{w}}} (p - p_0)\, \mathbf{n} \cdot \boldsymbol{\varphi}_l\ d\mathcal{S}(\mathbf{x}) \end{aligned} \tag{25}$$

Note that eqn. (24) represents a system of M linear ordinary differential equations for the modal amplitudes a_l, and can be written in matrix form as follows:

$$\underline{\ddot{\mathsf{a}}} + \Omega^2\, \underline{\mathsf{a}} = \underline{\mathsf{e}} \tag{26}$$

where:

$$(\Omega^2)_{ml} = \omega_m^2\, \delta_{ml}$$

In eqn. (26), the forcing term represents the coupling between the wall dynamics and the blood flow.

6 Fluid-wall interaction

Blood flow in arteries is pulsatile, with the fundamental frequency induced by the heart beat. The aim of the present work is to obtain the frequency-dependent transfer function of the fluid–structure interacting system, relating the inflow at $\mathcal{S}^{\mathsf{i}}$ to the velocity potential at arbitrary locations inside the arterial district. To accomplish this, the governing equations are rewritten in the frequency domain. By applying the Laplace transform to the eqns. (18) and (26), indicating with $\tilde{\cdot}$ the functions in frequency domain, we have:

$$\left(\frac{1}{2}\mathsf{I} - \mathsf{C}\right) \underline{\tilde{\phi}} = \mathsf{B}^{\mathsf{i}}\, \underline{\tilde{\chi}}^{\mathsf{i}} + \mathsf{B}^{\circ}\, \underline{\tilde{\chi}}^{\mathsf{or}} + (\mathsf{B}^{\circ}\mathsf{G} + \mathsf{B}^{\mathsf{w}})\, \underline{\tilde{\chi}}^{\mathsf{w}}. \tag{27}$$

and

$$s^2\, \underline{\tilde{\mathsf{a}}} + \Omega^2\, \underline{\tilde{\mathsf{a}}} = \underline{\tilde{\mathsf{e}}} \tag{28}$$

s being the Laplace variable. Note that eqn. (27) is formally identical to eqn. (18), and that the solution depends upon the frequency through the harmonic content of the forcing terms on the right hand side. This peculiarity is consistent with the assumption of incompressible fluid. Nevertheless, while in a rigid tube the propagation of the pressure perturbation is instantaneous in the flow field (and the fluid dynamic response has the same spectrum of the inflow), in the present formulation the term $\underline{\tilde{\chi}}^{\mathsf{w}}$ provides the coupling with the wall dynamics (eqn. (28)), through eqn. (19). Hence, the compliance of the vessel wall introduces a frequency dependent term in the dynamic response of the system.

The relationship between the velocity potential and the pressure perturbation is given by the Bernoulli theorem (eqn.(7)) which, in the frequency domain becomes:

$$\tilde{p} - \tilde{p}_0 = -s\,\rho\,\tilde{\phi}. \tag{29}$$

Substituting into eqn. (25) we obtain:

$$\tilde{e}_l = s\,\rho \int_{\mathcal{S}^{\mathrm{w}}} \tilde{\phi}\,\mathbf{n}\cdot\boldsymbol{\varphi}_l\,d\mathcal{S}(\mathbf{x}). \tag{30}$$

The velocity potential $\tilde{\phi}$ along the boundary $\mathcal{S}^{\mathrm{w}}$ is known from the piecewise–constant numerical solution of the system (27). Thus, the corresponding values of the generalized forces at those locations are obtained by considering the zeroth-order approximation for $\tilde{\phi}$ and by computing the inner product of eqn. (30) with a sum of N^{w} integrals on the panels, to have:

$$\tilde{e}_l \simeq s\,\rho \sum_{j=1}^{N^{\mathrm{w}}} \int_{\mathcal{S}_j^{\mathrm{w}}} \tilde{\phi}\,\mathbf{n}\cdot\boldsymbol{\varphi}_l\,d\mathcal{S}(\mathbf{x}) \simeq s\,\rho \sum_{j=1}^{N^{\mathrm{w}}} \tilde{\phi}_j \int_{\mathcal{S}_j^{\mathrm{w}}} \mathbf{n}\cdot\boldsymbol{\varphi}_l\,d\mathcal{S}(\mathbf{x}), \tag{31}$$

which is a linear representation of the l^{th} generalized force as a function of the value of the velocity potential on j^{th} panel. We define the matrix E such that:

$$\underline{\tilde{\mathsf{e}}} = s\,\rho\,\mathsf{E}\,\underline{\tilde{\phi}} \tag{32}$$

with

$$(\mathsf{E})_{lj} = \int_{\mathcal{S}_j^{\mathrm{w}}} \mathbf{n}\cdot\boldsymbol{\varphi}_l\,d\mathcal{S}(\mathbf{x}).$$

Substituting into eqn. (28) and solving with respect to $\underline{\tilde{\mathsf{a}}}$, one obtains:

$$\underline{\tilde{\mathsf{a}}} = s\,\rho\,\left(s^2\,\mathsf{I} + \Omega^2\right)^{-1}\,\mathsf{E}\,\underline{\tilde{\phi}} = \mathsf{H}(s)\,\underline{\tilde{\phi}}, \tag{33}$$

where H represents the $M \times N$ frequency-dependent matrix transfer function relating the velocity potential at the collocation points with the modal amplitude of the wall elastic displacement. Being $\underline{\tilde{\phi}}$ also evaluated on the sections $\mathcal{S}^{\mathrm{i}}$ and $\mathcal{S}^{\mathrm{o}}$, the matrix H is partitioned as:

$$\mathsf{H}(s) = \left[\begin{array}{ccccc} \mathbf{0} & \vdots & \hat{\mathsf{H}}(s) & \vdots & \mathbf{0} \end{array}\right]$$

where the submatrix $\hat{\mathsf{H}}(s)$ has dimension $M \times N^{\mathrm{w}}$.

Finally, to obtain the final form of the complete coupled fluid-wall dynamics, a relation between the wall motion and the boundary conditions of the flow is needed. To this aim, the modal representation of $\mathbf{u}$ into eqn. (19) yields:

$$\chi^{\mathsf{w}}(\mathbf{x},t) = \frac{d}{dt}\left[\sum_{m=1}^{M} a_m(t)\,\boldsymbol{\varphi}_m(\mathbf{x})\right]\cdot\mathbf{n} = \sum_{m=1}^{M} \dot{a}_m(t)\,\boldsymbol{\varphi}_m(\mathbf{x})\cdot\mathbf{n}.$$

Again, by means of the Laplace transform, we obtain, at the j^{th} collocation point:

$$\tilde{\chi}^{\mathsf{w}}_j = \sum_{m=1}^{M} s\,\tilde{a}_m\,\boldsymbol{\varphi}_m(\mathbf{x}_j)\cdot\mathbf{n}_j$$

or, in vector notation:

$$\underline{\tilde{\chi}}^{\mathsf{w}} = s\;\mathsf{R}\,\underline{\tilde{\mathsf{a}}} \tag{34}$$

with the generic entry of the $N \times M$ matrix given by:

$$(\mathsf{R})_{jm} = \begin{cases} \mathbf{n}_j\cdot\boldsymbol{\varphi}_m, & \mathbf{x}_j \in \mathcal{S}^{\mathsf{w}} \\ 0, & \text{otherwise} \end{cases}$$

The relationship between vectors $\underline{\tilde{\phi}}$ and $\underline{\tilde{\chi}}$ is obtained by combining the equations (33) and (34):

$$\underline{\tilde{\chi}}^{\mathsf{w}} = s\;\mathsf{R}\,\mathsf{H}(s)\,\underline{\tilde{\phi}}. \tag{35}$$

Substituting the relationship (35) into eqn. (18), the final fully–coupled system of equations is:

$$\left(\frac{1}{2}\mathsf{I} - \mathsf{C}\right)\underline{\tilde{\phi}} = \mathsf{B}^{\mathsf{i}}\underline{\tilde{\chi}}^{\mathsf{i}} + \mathsf{B}^{\mathsf{o}}\underline{\tilde{\chi}}^{\mathsf{or}} + s\,(\mathsf{B}^{\mathsf{o}}\mathsf{G} + \mathsf{B}^{\mathsf{w}})\mathsf{R}\,\mathsf{H}(s)\underline{\tilde{\phi}}$$

which, solved for $\underline{\tilde{\phi}}$, gives:

$$\underline{\tilde{\phi}} = \left[\frac{1}{2}\mathsf{I} - \mathsf{C} - s\,(\mathsf{B}^{\mathsf{o}}\mathsf{G} + \mathsf{B}^{\mathsf{w}})\mathsf{R}\,\mathsf{H}(s)\right]^{-1}\left[\mathsf{B}^{\mathsf{i}}\underline{\tilde{\chi}}^{\mathsf{i}} + \mathsf{B}^{\mathsf{o}}\underline{\tilde{\chi}}^{\mathsf{or}}\right] = \mathsf{T}(s)\,\underline{\tilde{\mathsf{q}}} \tag{36}$$

where

$$\mathsf{T}(s) = \left[\frac{1}{2}\mathsf{I} - \mathsf{C} - s\,(\mathsf{B}^{\mathsf{o}}\mathsf{G} + \mathsf{B}^{\mathsf{w}})\mathsf{R}\,\mathsf{H}(s)\right]^{-1}$$

is the frequency–dependent matrix transfer function relating the known flux $\underline{\tilde{\mathsf{q}}}$ through $\mathcal{S}^{\mathsf{i}}$ and $\mathcal{S}^{\mathsf{o}}$, with the velocity potential on $\mathcal{S}$. Note that T includes the effects of the wall dynamics through the matrix H.

7 Numerical results

Numerical experiments are carried out to validate the above formulation. Although this is applicable for three dimensional analysis of arbitrarily shaped arterial districts, in this section the attention is limited to straight thin-walled cylindrical vessels. In the following subsection a specific expression for the structural model is given, as well as the form of the eigenfunctions φ_m corresponding to the boundary conditions chosen. In subsection 7.2 the procedure used to numerically evaluate the input impedance of the vessel is outlined and, in subsections 7.3 and 7.4, the results of the convergence analysis and a preliminary simulation are presented.

7.1 The elastic wall operator

Arterial tissues are characterized by a rather complex structure, and experimental studies have demonstrated that they deform orthotropically. Several constitutive nonlinear models have been proposed to describe the strain-stress relationship of the vascular wall [11], [12]. On the other hand, it has been observed that the assumption of small elastic deformations around a reference configuration is reasonable, and the structural dynamics may be represented with an acceptable level of approximation using a linear model.

In this work, we adopt one of these models, assuming the vessel wall to behave like a purely elastic membrane [2],[18]. Despite its simplicity, the proposed formulation is able to predict the propagation velocity of pressure perturbations with good accuracy, since it has been demonstrated that the effects of the viscous dissipation play only a secondary role in the local wave propagation mechanism [1]. Therefore, a purely elastic model is appropriate for the study of local variations in the wave speed, due to local inhomogeneity of the elastic wall and/or geometric variation of the vessel cross section, such as prosthetic implantations, atherosclerotic plaques, stenoses, etc.

Let us assume a straight cylindrical arterial segment of length L having a circular cross section of reference radius R_0. Considering a cylindrical coordinate system (x, θ, r) (fig. 3), we denote with u and w the components of the elastic displacement $\mathbf{u}$ in the longitudinal and radial directions respectively. The hypotheses we are dealing with are: *(i)* incompressible isotropic elastic material characterized by a single value for the Young modulus E and the Poisson's ratio ν; *(ii)* wall thickness $h \ll R_0$; *(iii)* $w \ll R_0$. By neglecting the elastic deformations in the azimuthal direction, the membrane equations governing the structural dynamics are [2],[5]:

$$\begin{cases} \rho_{\mathrm{w}} h \dfrac{\partial^2 u}{\partial t^2} &= \dfrac{Eh}{1-\nu^2}\left(\dfrac{\nu}{R_0}\dfrac{\partial w}{\partial x} + \dfrac{\partial^2 u}{\partial x^2}\right) + f_u \\ \rho_{\mathrm{w}} h \dfrac{\partial^2 w}{\partial t^2} &= kG_s h \dfrac{\partial^2 w}{\partial x^2} - \dfrac{Eh}{1-\nu^2}\left(\dfrac{\nu}{R_0}\dfrac{\partial u}{\partial x} + \dfrac{w}{R_0^2}\right) + f_w \end{cases} \tag{37}$$

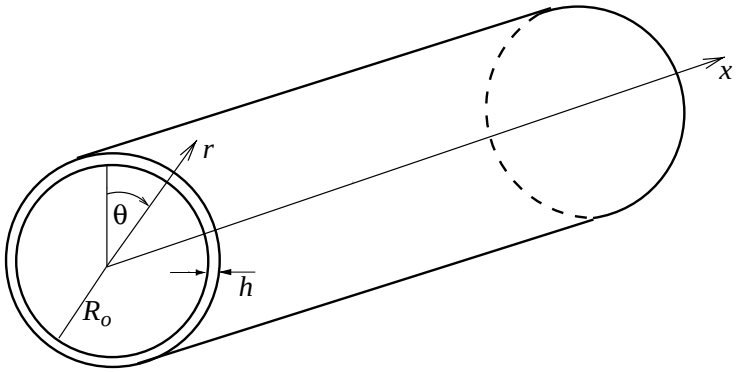

Figure 3: The cylindrical straight tube and the coordinate system.

where, G_s is the shear modulus, k is the Timoshenko's shear correction factor [18], f_u and f_w represent the forcing terms due to the action of the blood flow. The inviscid fluid model implies $f_u = 0$. Assuming a negligible longitudinal deformation u, eqn. (37.1) is automatically satisfied, to yield:

$$\rho_{\mathrm{w}} h \frac{\partial^2 w}{\partial t^2} = k G_s h \frac{\partial^2 w}{\partial x^2} - \frac{Eh}{1-\nu^2}\frac{w}{R_0^2} + f_w \tag{38}$$

The above differential equation for w is formally identical to the equation governing the motion of a vibrating string lying on an elastic soil. The transverse elastic effect is produced by the radial displacement (second term on the right hand side of eqn. (38)), and represents the contribution of the restoring force due to the deformation of the annular sections of the vessel. Hence, the linear structural operator (per unit thickness) used here has the following form:

$$\mathcal{L} = -k G_s \frac{\partial^2}{\partial x^2} + \frac{E}{(1-\nu^2)\, R_0^2}\mathcal{I} \tag{39}$$

where $\mathcal{I}$ is the identity operator (cfr. eqn. (20)). To obtain the eigenfunctions of $\mathcal{L}$, we need boundary conditions for the elastic displacements. Here, we assume hinged conditions for the limit sections of the vessel, *i.e.*, $w(0,t) = w(L,t) = 0$. These boundary conditions are not suitable to study the behaviour of an *in vivo* arterial district, but may be useful to compare the numerical results to *in vitro* experiments available in the literature, and lead a simple form for the eigenfunctions $\boldsymbol{\varphi}_m$. In addition, they allow for an easy evaluation of the wave velocity from the resonance frequencies of the system and constitute a useful benchmark to assess the methodology. The eigenvalue problem (21) becomes:

$$\frac{\partial^2 \boldsymbol{\varphi}_m}{\partial x^2} + \mu_m^2\, \boldsymbol{\varphi}_m = 0 \tag{40}$$

where

$$\mu_m^2 = \frac{\lambda_m \rho_{\mathrm{w}}}{k G_s} - \frac{E}{k G_s (1-\nu^2) R_0^2}$$

The general solution of eqn. (40) is: $\varphi_m(x) = A\cos(\mu_m x) + B\sin(\mu_m x)$.

Imposing $\varphi_m(0) = \varphi_m(L) = 0$ we obtain:

$$\varphi_m(x) = \sin\left(\frac{m\,\pi\,x}{L}\right)$$

with the corresponding eigenvalue:

$$\lambda_m = \frac{k G_s}{\rho_{\mathrm{w}}}\left[\left(\frac{m\pi}{L}\right)^2 + \frac{E}{k G_s (1-\nu^2) R_0^2}\right]$$

7.2 The input impedance

In this work we focus our attention on the harmonic response of the coupled fluid-structure system, being the wall dynamics typically driven by a pulsatile inflow. As we will see later, the phase wave velocity may be derived from its resonance frequencies, which correspond to the peaks of the response spectrum. To characterize the harmonic behaviour of the system, a suitable quantity is represented by the *input impedance* of the arterial segment [1]:

$$\tilde{Z}^{\mathrm{i}}(s) = \frac{\tilde{p}(s) - p_0}{\mathbf{v}^{\mathrm{i}}(s)\cdot\mathbf{n}}. \tag{41}$$

It can be considered as the transfer function relating the pressure perturbation at $\mathcal{S}^{\mathrm{i}}$ and the flow through it. Under the assumption introduced in the present study, eqn. (41) is rewritten as:

$$\tilde{Z}^{\mathrm{i}}(s) = \frac{-s\,\rho\,\tilde{\phi}^{\mathrm{i}}(s)}{\tilde{\chi}^{\mathrm{i}}(s)} \tag{42}$$

where $\tilde{\chi}^{\mathrm{i}}(s)$ is assumed a given function. To numerically evaluate the input impedance of the compliant vessel the following procedure is used: first, the system is forced with a periodic inflow oscillating at a specified frequency ω_q; then, the solution of the problem is obtained on the entire boundary $\mathcal{S}$; finally, $\tilde{Z}^{\mathrm{i}}$ is computed by averaging the value defined in eqn. (42) on $\mathcal{S}^{\mathrm{i}}$,

$$\tilde{Z}^{\mathrm{i}}(\omega_q) = \frac{-j\,\omega_q\,\rho}{\mathcal{A}^{\mathrm{i}}}\int_{\mathcal{S}^{\mathrm{i}}} \frac{\tilde{\phi}(\mathbf{x},\omega_q)}{\tilde{\chi}(\omega_q)}\,d\mathcal{S}(\mathbf{x}) \tag{43}$$

To analyze the harmonic response of the system, the frequency range of interest is spanned by forcing the system with a periodic inflow with constant amplitude *i.e.*, $\tilde{\chi}^{\mathrm{i}}(\omega) = 1$. The resulting spectrum $\tilde{Z}^{\mathrm{i}}(\omega)$ is used to get the resonance frequency by identifying the location of its peaks.

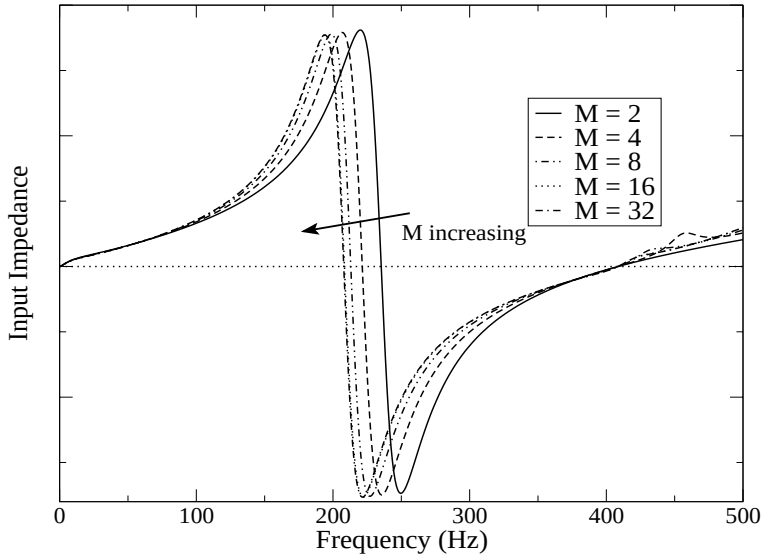

Figure 4: Spectrum of the input impedance imaginary part $\Im[\tilde{Z}^{i}(\omega)]$ (length $L = 1\ m$, reference radius $R_0 = 1\ cm$, Young modulus $E = 6 \times 10^7\ Pa$, wall density $\rho_w = 1030\ Kg/m^3$, fluid density $\rho = 51\ Kg/m^3$). The parametric analysis is made with respect to the number of eigenfunctions.

The wave propagation velocity is derived through the well known similarity with an equivalent one-dimensional acoustic problem [1]: let us consider a rigid pipe of length L closed at both ends and filled with a compressible fluid, with speed of sound c. The air column enclosed resonates at frequencies given by:

$$f_k = \frac{c}{\gamma} = \frac{k\,c}{2\,L} \qquad\qquad k = 1, 2, ... \tag{44}$$

where γ is the wavelength of the travelling wave. Since the boundary conditions at the input and output sections of the vessel segment satisfy this assumption, eqn. (44) may be used to evaluate c from the resonance frequencies. To validate the wave velocity obtained with the above technique, the results of the present method will be compared to the well assessed Moens-Korteweg formula [1], in the modified form due to Bergel [19]. According to such a model, the relationship between the propagation velocity of a pressure perturbation and the elastic wall properties is given by:

$$c = \sqrt{\frac{E\,h}{2\,\rho\,R_0(1-\nu^2)}} \tag{45}$$

7.3 Convergence analysis

The above formulation is affected by two numerical approximations: the boundary element representation of the boundary $\mathcal{S}$, depending on the number of panels N, and the truncation order M of the modal expansion of the elastic wall displacement w. The effect of these two parameters is deeply correlated by eqn. (28) and eqn. (34), used to evaluate the coupling terms. In particular, the number of collocation points along S^{w} should be sufficiently large to properly capture pressure fluctuations up to the wavelength of the highest mode considered.

In fig. 4 the spectrum of the imaginary part of the input impedance for several values of M is shown. The cylindrical tube is 1 m long, with $R_0 = 1$ cm, to simulate a one-dimensional problem. We used non–physical values for fluid density ρ and Young's modulus E, to obtain an expected value for the wave velocity of the same order of magnitude of that of the sound in the air, and spectrum characteristics comparable to those of a resonating pipe. The number of panels used is $N^{\mathrm{w}} = 180$. Figure 4 includes the impedance spectrum predicted by successive doubling of the number of fundamental modes, from 2 up to 32, in a frequency range surrounding the first resonance. The value predicted by the Moens–Korteweg–Bergel formula is $c = 396$ m/s, corresponding to the eigenfrequency $f_1 = 198$ Hz. The result converges monotonically towards such a reference value. The spectra corresponding to the two highest truncation orders (16 and 32) are

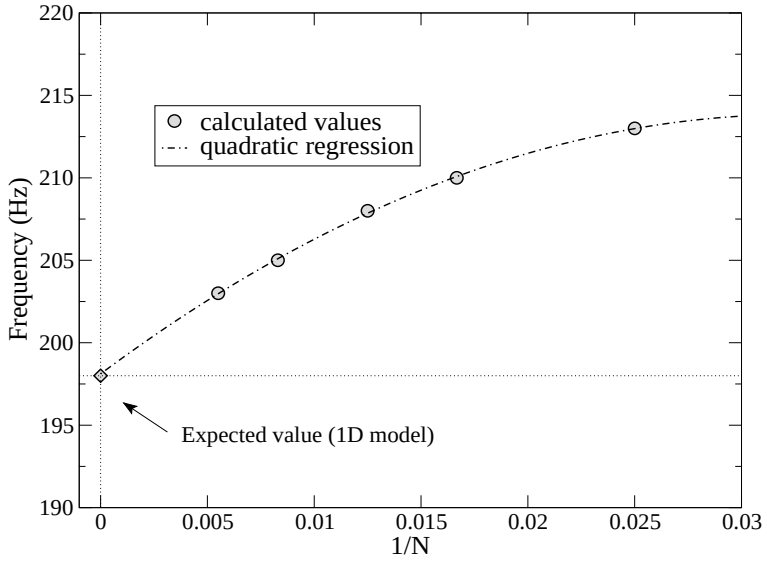

Figure 5: First resonance frequency vs. the number of panels N. The asymptotic estimate for $N \to \infty$ is obtained by extrapolation of a quadratic regression of the data, and it is compared to the value predicted by the 1D model. Same test case of Fig. 4.

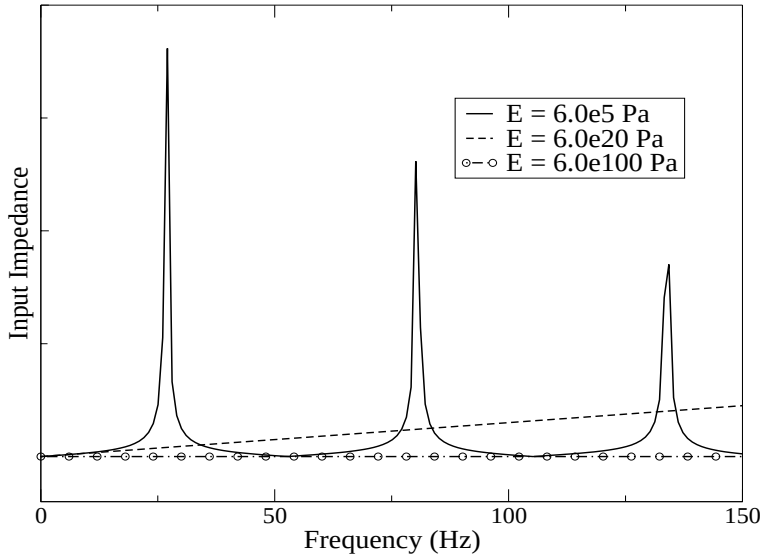

Figure 6: Amplitude spectrum of the input impedance. Parametric analysis is made with respect to the Young modulus E. Same test case of Fig. 4.

almost identical, revealing that the solution converges for a truncation order lower than the maximum limit allowable by the BEM mesh used (for a proper evaluation of E, we set a lower limit of five collocation points for each wavelength).

Nevertheless, the eigenfrequency evaluated with 32 modes is still above $200\,\mathrm{Hz}$. To completely assess the convergence of f_1 to the expected value, it is necessary to verify the influence of the BEM mesh on the solution, at a given M. Figure 5 depicts the value of the first resonance as a function of $1/N$ (for $M = 32$). The computed values are fitted by means of a second-order regression, and the asymptotic estimate of the solution for $N \to \infty$ is obtained by extrapolation. The agreement with eqn. (45) is excellent (diamond symbol), revealing the capability of the method to reproduce accurately the well assessed Bergel's model.

We complete the parametric analysis by investigating the effect of the wall stiffness on the solution. From eqn. (45) it is evident that the wave phase velocity increases with the square root of the Young's modulus. In the rigid wall limit ($E \to \infty$), any perturbation propagates instantaneously (for incompressible fluids) in the whole fluid domain, and the relationship between the inflow and the outflow reduces to the frequency–independent ratio $\mathcal{A}^{\circ}/\mathcal{A}^{\mathrm{i}}$. Figure 6 shows the results of this parametric study. The amplitude spectrum of the input impedance for the $1\,\mathrm{m}$ long tube shows the correct trend for increasing values of the Young's modulus. In particular, for $E = 6 \times 10^{100}$ Pa, the frequency response of the system is zero in the whole frequency range, which is compatible with the expected behaviour of an incompressible fluid flowing inside a rigid pipe.

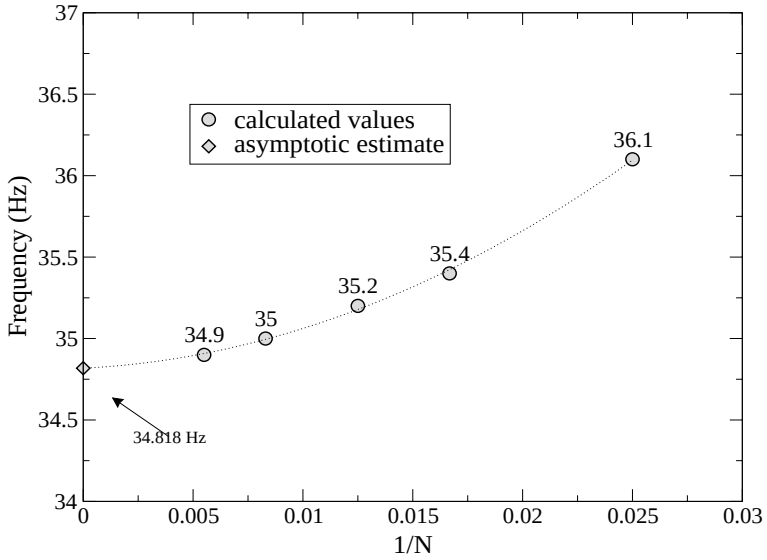

Figure 7: Asymptotic $1/N$ convergence of the first resonance frequency for an arterial district (length $L = 0.1$ m, radius $R_0 = 1$ cm, Young modulus $E = 6 \times 10^5$ Pa, fluid density $\rho = 1000\,\mathrm{Kg/m^3}$, wall density $\rho_w = 1030\,\mathrm{Kg/m^3}$). The corresponding estimated wave velocity is 6.978 m/s .

7.4 A realistic case study

To complete the preliminary assessment of the proposed method, we attempt the simulation of blood flow in a simple arterial district, characterized by physiological values for the Young's modulus, Poisson's ratio, wall and fluid densities. The test case corresponds to $L = 10$ cm, with radius $R_0 = 1$ cm and wall thickness $h = 1$ mm. The density of the fluid is $\rho = 1000\,\mathrm{Kg/m^3}$, and $\rho_w = 1030\,\mathrm{Kg/m^3}$. Figures 7 and 8 show the result obtained for such a case study. First, we fix the Young's modulus ($E = 6 \times 10^5$ Pa) and examine the variation of the first resonance frequency of the vessel. Using the same approach described in subsection 7.3, we evaluate the asymptotic value by extrapolation of the data in the limit $N \to \infty$. This limit value is used to compute the wave speed in the artery by means of eqn. (44). The estimated propagation velocity is 6.98 m/s, in agreement with the physiological value.

To go one step further, we repeated the above procedure for different values of the wall stiffness E, in the range of variation typical of human healthy vessels. The results are presented in fig. 8, where the value of the wave velocity is plotted as a function of E. The computed velocities are in good agreement with the expected values [1], and suggest that the proposed methodology may be considered as a promising tool for the evaluation of the wave propagation speed inside compliant vessels.

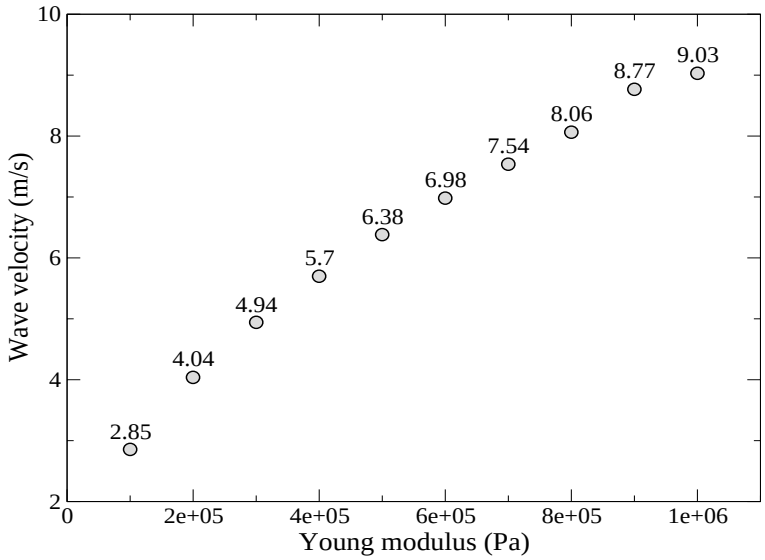

Figure 8: Influence of the Young modulus on the computed wave velocity for the same test case as Fig. 7.

8 Conclusions

Mathematical models predicting the wave propagation characteristics (such as velocity and impedance) of an arterial vessel are of interest for the clinicians. The outcome of such models constitute physiological indicators of diagnostic significance and their anomalies can be used to detect pathological states in the vascular system. In this chapter, a boundary element method has been presented and developed for studying the wave propagation phenomena in an artery. This formulation is based on the intrinsic coupling between a boundary integral representation of the flow equations and the vessel wall dynamics. Another advantage of the presented methodology is the possibility to analyze complex three dimensional geometries. Preliminary numerical results in a basic configuration show the capability of the method of predicting the relevant propagation features, with a modest computational effort. Though some hypothesis have been included for simplicity, the integral formulation can be extended to a variety of other possible cases. In particular, the influence of the wall viscoelasticity can be easily investigated. Moreover, a time domain analysis is worth accomplishing to include other effects such as the fluid viscosity.

Acknowledgments
The authors greatly acknowledge the fruitful discussions with Prof. L. Morino.
This work has been supported by the CNR program *Agenzia2000*
n. CNRC00A3F1_002, 2001.

References

[1] Milnor, W.R., *Hemodynamics*, William & Wilkins, Baltimore/London, 1982.

[2] Quarteroni, A., Tuveri, M. & Veneziani, A., Computational vascular fluid dynamics: problems, models and methods, *Comp. Vis. Science*, **2**, pp. 163-197, 2000.

[3] Pontrelli, G. & Rossoni, E., Numerical modelling of the pressure wave propagation in the arterial flow, *Int. J. Num. Meth. Fluids*, **43(6)**, in press, 2003.

[4] Tijsseling, A.S., Fluid-structure interaction in liquid filled pipe systems: a review, *J. Fluids and Structures*, **10**, pp. 109-146, 1996.

[5] Nobile, F., *Numerical approximation of fluid-structure interaction problems with application to haemodynamics*, Ph. D. These n. 2458, EPFL (Lausanne), 2001.

[6] Morino, L., Boundary integral equations in aerodynamics, *Appl. Mech. Rev.* **46 (8)**, pp. 445-466, 1993.

[7] Morino, L., Is there a difference between aeroacoustics and aerodynamics? An aeroelastician's point of view, *AIAA journal*, in press, 2003.

[8] Iemma, U., BEM simulation of woodwind musical instruments, in 7^{th} *International Congress on Sound and Vibration*, Garmish-Partenkirchen, Germany, July 2000.

[9] Iemma, U. & Gennaretti, M., Integrated aeroacustoelastic modelling for the analysis of the propeller-driven cabin noise, *AIAA Paper 99-1919*, 1999.

[10] Iemma, U., Morino, L. & Trainelli, L., Internal noise generated by sources external to an elastic shell, *AIAA Paper n. 95-042*, 1995.

[11] Zhou, J. & Fung, Y.C., The degree of nonlinearity and anisotropy of blood vessel elasticity, *Proc. Natl. Acad. Sci. USA*, **94**, pp. 14255-14260, 1997.

[12] Schulze-Bauer, C.A.J. & Holzapfel, G.A., Determination of constitutive equations for human arteries from clinical data, *J. Biomech.* **36 (2)**, pp. 165-169, 2003.

[13] Kress, R., *Linear Integral Equations*, Springer & Verlag, Berlin, 1989.

[14] Rienstra, S.W. & Hirschberg A., *An Introduction to Acoustics*, Eindhoven University of Technology, IWDE Report 92-06, 2001.

[15] Crighton, D.G., Dowling, A.P., Ffowcs Williams, J.E., Heckl, M. & Leppington, F.G., *Modern Methods in Analytical Acoustics - Lecture Notes*, Springer–Verlag, New York, 1992.

[16] Morino, L. & Tseng, K., A General Theory for Unsteady Compressible Potential Flows with applications to Aeroplanes and Rotors, in *Boundary Elements Method In Nonlinear Fluid Dynamics, Developments in Boundary Elements Methods*, Banerjee and Morino Eds., pp. 183-245, Elsevier App. Sci., 1990.

[17] Iemma, U., Marchese, V. & Morino, L., Higher–Order BEM For Potential Transonic Flows, *Comp. Mech.*, **21 (3)**, pp. 243-252, 1998.
[18] Timoshenko, S., *Theory of plates and shells*, McGraw-Hill , New York, 1940.
[19] Bergel, D.H., The dynamic elastic property of the arterial wall, *J. Physiol.*, **156**, pp. 458-469, 1961.